The catalytic pocket of the ring-hydroxylating dioxygenase from Sphingomonas CHY-1

Jean Jakoncic, Yves Jouanneau, Christine Meyer, V. Stojanoff

The catalytic pocket of the ring-hydroxylating dioxygenase from *Sphingomonas* CHY-1

Jean Jakoncic[1], Yves Jouanneau[2], Christine Meyer[2], Vivian Stojanoff[1]

[1]Brookhaven National Laboratory, National Synchrotron Light Source, Upton, NY 11973, USA

[2]Laboratoire de Biochimie et Biophysique des Systèmes Intégrés, CEA, DSV, DRDC and CNRS UMR 5092, CEA-Grenoble, F-38054 Grenoble Cedex 9, France.

Corresponding author:

Vivian Stojanoff

Brookhaven National Laboratory

Upton NY 11973 US

Tel. : 1 631 344 8375; Fax : 1 631 344 3238

Email : vivian.stojanoff@gmail.gov

Abstract

Ring-hydroxylating dioxygenases are multicomponent bacterial enzymes that catalyze the first step in the oxidative degradation of aromatic hydrocarbons. The dioxygenase from *Sphingomonas* CHY-1 is unique in that it can oxidize a wide range of polycyclic aromatic hydrocarbons (PAHs). With a crystal structure similar to that of the seven other known dioxygenases, its catalytic domain features the largest hydrophobic substrate binding cavity characterized so far. Molecular modeling studies indicated that the catalytic cavity is large enough to accommodate a five-ring benzo[a]pyrene molecule. The predicted positions of this and other PAHs in the substrate binding pocket are consistent with the product regio- and stereo-selectivity of the enzyme.

Keywords: dioxygenase; catalytic domain; mononuclear iron; bioremediation; high molecular weight polycyclic aromatic hydrocarbons

The first step in the biodegradation of aromatic hydrocarbons by aerobic bacteria often involves a dihydroxylation on two adjacent carbon atoms of the aromatic ring, catalyzed by a ring-hydroxylating dioxygenase (RHD). RHDs form a large family of enzymes, very diverse in terms of substrate specificity and protein sequence [1]. Their role is crucial in the degradation of many organic pollutants, including polycyclic aromatic hydrocarbons (PAHs), which are notorious for their resistance to biodegradation. Several bacteria were found to degrade PAHs but only a few have been reported to attack four and five ring PAHs [2,3]. In *Sphingomonas* strain CHY-1 a single RHD has been shown to be responsible for the oxidation of a wide range of PAHs [4]. This dioxygenase consists of three components, a NADH-dependent reductase (PhnA4), a ferredoxin containing a Rieske type [2Fe-2S] cluster (PhnA3), and a terminal oxygenase, PhnI, containing both a mononuclear iron [Fe^{2+}] and a [2Fe-2S] Rieske cluster [5]. Recent biochemical studies showed that the dioxygenase from strain CHY-1 was able to oxidize at least eight PAHs made of 2 to 5 aromatic rings, in contrast to most other dioxygenases, whose selectivity is limited to 2 and 3 ring PAHs [6,7,8]. A positive electron density observed in the PhnI refined three-dimensional structure served as probe in modeling different substrates in the catalytic pocket. This study presents evidence that the broad substrate specificity of the enzyme is primarily due to the large volume and particular shape of its catalytic pocket.

Material and Methods

The purification of recombinant His-tagged PhnI was performed as described previously [5]. The protein was further purified by gel filtration chromatography following His-tag removal by thrombin cleavage. Crystals were grown at room temperature using the sitting drop method and a crystallization solution derived from Cryoscreen solution 67 (Nextal Biotechnologies, Montreal, Quebec, CA). Crystals that diffracted up to 1.85 Å resolution (Jakoncic, unpublished work) were obtained by further covering each well with mineral oil [9]. Diffraction data were recorded on beam line X6A at the National Synchrotron Light Source [10]. The 3D structure was determined by molecular replacement, using the α-subunit from naphthalene dioxygenase from *Pseudomonas* sp. Strain NCIB 9816-4, NDO-$O_{9816\text{-}4}$ [6] and the β-subunit from cumene dioxygenase from *P. fluorescens* strain IP01, CDO-O_{IP01} [11] as templates. The model was refined using REFMAC [12] and COOT [13] to R and R_{free} factors of 19.7 and 23.6 %, respectively (Fig. 1). Most of the amino acids are present in the final model (PDB accession code 2CKF), with the exception of residues in the C- and N- termini regions and a highly flexible region at the entrance of the catalytic pocket LI (residues 221 to 240) and LII (residues 253 to 265) described in the following section.

Results and Discussion

The PhnI catalytic domain. The PhnI quaternary and tertiary structures were found to be similar to those of other RHDs, featuring a $\alpha_3\beta_3$ arrangement with each αβ heterodimer (Fig. 1) related to the other by a non-crystallographic three-fold axis [6]. Each α-subunit can be divided into a Rieske-cluster containing domain and a catalytic domain

hosting one mononuclear iron. The core region of the catalytic domain is dominated by a nine-stranded anti-parallel β-sheet that divides the domain into two parts: the active site of the enzyme on one side of the β-sheet and the Rieske domain on the other. Strategically located in the vicinity of the catalytic iron atom, and covering one side of the sheet, lies a highly conserved secondary structure amongst RHDs, a α-helix that extends from residues 336 to 373 in PhnI. The mononuclear Fe atom is located in the center of a 35 Å long cavity extending from the solvent to the anti-parallel β-sheet. On one side of the cavity, a hydrophobic pocket extends from the solvent to the mononuclear iron (Fig. 1). Two solvent exposed loops, LI and LII, form the entrance of the pocket. The overall temperature factor of the Cα main chain in this region is relatively higher compared to the rest of the molecule; the B factor being highest for LI. While LI was relatively well defined in one of the α monomers with only five missing amino acids (Fig.1), it was barely detectable in the other two. LII on the other hand was fully defined in the electron density maps, but presented a different conformation for each of the monomers. Highly flexible structures are also observed in the corresponding regions for other RHDs, suggesting that LI might control the access to the catalytic pocket.

In the PhnI crystal structure, an unidentified ligand could be observed in two of the three catalytic pockets. As shown in Fig. 2, the size and shape of the density recalls that of an indole molecule with its C3 carbon located 4.5 Å from the catalytic iron atom. The electron density maps in Fig. 2 clearly show the presence of a residual positive density between the catalytic iron and the modeled indole molecule. Therefore the final PhnI crystal model only includes two water molecules in this region.

The catalytic pocket. The Phn1 catalytic pocket has a trapezoidal shape, wider at the entrance (close to the solvent) and narrower towards the catalytic Fe atom. The average dimensions are 12 Å in length, 8 Å in height and 5.5 to 6.5 Å in width. The program POCKET [14] was employed to determine the volume of the PhnI substrate binding pocket. The resulting volume corresponds to the unoccupied space determined by a 1.4 Å radius probe following the protein surface. The mononuclear iron and its three ligands, His 207, His 212 and Asp 360, as well as, the coordinated water molecules, were not included for the calculations. For comparison purposes, the volume of the catalytic pocket was also determined for two other dioxygenases in their substrate free form. The smallest pocket size with an estimated volume of 45 $Å^3$ was determined for biphenyl dioxygenase from *Rhodococcus* sp. Strain RHA1, BPDO-O_{RHA1} (PDB access code 1ULI) [15], while the catalytic pocket volume for naphthalene dioxygenase, NDO-O_{9816} (PDB access code 1NDO) [6], found to be 65 $Å^3$, is significantly larger. The Phn1 catalytic pocket, with its 91 $Å^3$, is the largest reported so far. Compared to the substrate free form of NDO-O_{9816} and BPDO-O_{RHA1} the PhnI catalytic pocket is at least 2 Å longer, wider and higher at the entrance in the solvent region, which would likely explain the ability of this enzyme to oxidize larger PAH substrates with up to 5 rings [5]. The structural determination of the BPDO-O_{RHA1} enzyme in the presence of its substrate showed that the catalytic pocket becomes 1.5 Å longer compared to the substrate-free enzyme [15]. The α-helix, containing residues Leu 274 and Ile 278 (Leu 223 and Ile260 in Phn1), is translated about 1.4 Å towards the solvent upon binding the biphenyl molecule, thereby increasing the pocket length. A similar translation was observed for 2-Oxoquinoline 8-Monooxygenase from *Pseudoomonas putida* 86, OMO-O_{86}, where the loop at the entrance of the catalytic pocket

(equivalent to loop LI in PhnI) underwent a significant conformational change upon substrate binding [16].

Sequence identity of structurally analogous residues lining the catalytic pocket for different dioxygenases of known crystallographic structure shows that PhnI presents the highest sequence identity with NDO-O_{9816} and the lowest with carbazole-1-9α- dioxygenase from *P. resinovorans* strain CA10 (CARDO-O_{CA10}) [17]. The classification presented in Table 1, based on α-subunit sequence homology and substrate specificity, is consistent with current classifications [18]. The PhnI catalytic pocket represented in Fig. 3 can be divided into three regions, distal, central and proximal, depending on the distance to the mononuclear Fe atom (Table 1). Compared to other dioxygenases, the PhnI pocket is rather uniform in shape and does not present any kinks or torsions as was found for example for BPDO-O_{RHA1} [15]. Residues Phe 350 and Phe 404 in the central region are expected to affect the topology of the catalytic pocket and consequently select the shape and form of allowed substrates. Accordingly, the replacement of Phe 352 in NDO-$O_{9816\text{-}4}$ by smaller amino acids significantly altered the regiospecifity of the reaction products [19]. In NDO-$O_{9816\text{-}4}$ Phe 404 is replaced by Ala 407. Further differences, observed at positions 308 and 356, contribute to enlarge the catalytic pocket of PhnI compared to that of NDO-$O_{9816\text{-}4}$. Indeed, Leu 356 in PhnI is replaced by a bulky aromatic residue (Trp or Phe) in naphthalene dioxygenases (Table 1).

Residues in the distal region seem to exert a greater influence in selecting the size and shape of allowed substrates. In PhnI, most significant are residues Leu 223 and Leu 226 located on loop LI, and residues Ile 253 and Ile 260 on loop LII. In naphthalene dioxygenases, NDO-O_{9816} and NDO-O_{12038}, Leu 223, is substituted by a bulkier and less

flexible phenylalanine residue (Table I). The diversity in residues structurally equivalent to Ile 260 in PhnI must relate to the different substrate specificity observed between the members of the naphthalene dioxygenase family.

Substrate specificity. To explore the substrate specificity of PhnI from a structural point of view, 2, 3, 4 and 5 ring PAHs were modeled into the catalytic pocket of the refined structure (PDB access code 2CKF). The structures of the enzyme-substrate complexes described for NDO-O_{9816} and BPDO-O_{RHA1} (PDB access codes 1O7G and 1ULJ), were first used to fit and adjust the position of naphthalene and biphenyl substrates in the PhnI catalytic pocket. As the pocket is narrower in the proximal region (Fig.4), modeling indicated that the two-ring substrates would be locked in a single position consistent with the finding that PhnI hydroxylates naphthalene and biphenyl, respectively, in positions 1,2- and 2,3- [5]. Phenanthrene, a three ring angular molecule, could theoretically be hydroxylated in positions 1,2-, 3,4-, or 9,10-. However, due to steric constraints imposed by the PhnI pocket, only one position, which would bring the C3 and C4 carbon atoms close to the active Fe atom site, is allowed. This analysis corroborates enzymatic assays for which *cis*-3,4- phenanthrene dihydrodiol was the only product detected [5].

The five ring PAH benzo[a]pyrene can only fit into the PhnI catalytic pocket in a single orientation. Minor conformational changes are assumed in modeling indicating that the side chains of Leu 223 and Phe 350 need to be rotated if the substrate is to fit in the pocket. In this orientation, shown in Fig. 4, benzo[a]pyrene would be hydroxylated in position 9,10-. In fact 9,10-*cis*-dihydrodiol- benzo[a]pyrene is the only product observed as the

result of enzymatic assays [5]. On the other hand, benzo[a]anthracene (BaA), a four ring PAH, was found to be attacked at positions 1,2-, 8,9- and 10,11- with *cis*-dihydrodiols 1,2- and 10,11- presenting the highest yields. Substrate orientation leading to an hydroxylation on the 1,2- position would require a minimal rearrangement of residues in the catalytic pocket, involving only side chain conformational changes of Leu 223 in loop LI. Hydroxylation on carbons C10 and C11 would occur for a position of the substrate requiring rearrangements of both Leu 223 and Phe 350 side chains. Conformational changes of residues 223, 253 and 404 should take place to allow hydroxylation of BaA at the less favorable 8,9- position. These predictions are in accordance with the catalytic properties of the enzyme, since it was found to produce much less of the 8,9-dihydrodiol [5].

Phe 350 and Phe 404 in the central region contribute to the regio-specificity and to the PhnI pocket shape. Phe 350 is conserved in NDO-$O_{9816\text{-}4}$ and in the naphthalene dioxygenase from *Rhodococcus* sp. strain NCIMB 12038 (NDO-O_{12038}) [7], while Phe 404 is replaced by Ala 407 in NDO-$O_{9816\text{-}4}$ and by Asp 418 in NDO-O_{12038}. In NDO-$O_{9816\text{-}4}$, mutations of Phe 352 (Phe 350 in PhnI) into a valine and a leucine resulted in altered regio-specificity of the enzyme. These mutations altered the pocket topology, so that other orientations of the biphenyl and phenanthrene substrates were allowed [20]. The pocket size and shape might also influence the effectiveness of the reaction, by locking the substrate in the right position before catalysis. Replacement of Trp 358 by an alanine in NDO-O_{12038} resulted in inefficient transformation of naphthalene, because the bulky side chain of Trp 358 was crucial to maintain the substrate in the right position [19]. It is

interesting to note all RHDs of known structure have an aromatic residue at a position equivalent to Trp 358, except PhnI, which has a leucine in the corresponding position.

In conclusion, PhnI is endowed with a remarkable broad specificity towards high molecular weight PAHs, which might be explained by the shape and size of its substrate binding pocket. The PhnI pocket was found to be at least 2 Å longer and wider at the entrance a unique feature between dioxygenases of known structures certainly allowing the five-ring benzo[a]pyrene to bind to the catalytic Fe. Modeling of various PAHs showed that Phe 350 in the central region of the pocket is essential for the regio- and substrate specificity, while Leu 223 and Ile260 in the distal region contribute to the specificity of high molecular weight PAHs. Further studies involving replacements of specific residues of the substrate-binding pocket by site-directed mutagenesis should bring new insights into the role of these residues in the catalytic activity of the enzyme.

Acknowledgements

We would like to thank the staff of the National Synchrotron Light Source, Brookhaven National Laboratory for their continuous support. The NSLS is supported by the U.S. Department of Energy, Office of Science, Office of Basic Energy Sciences, under Contract No. DE-AC02-98CH10886. The NIGMS East Coast Structural Biology Facility, the X6A beam line, is funded under contract # GM-0080.

References

[1] C.S. Butler, J.R., Mason, Structure–function analysis of the bacterial aromatic ring-hydroxylating dioxygenases, Adv. Microb. Physiol. 38 (1997) 47-84.

[2] A.L. Juhasz, R. Naidu, Bioremediation of high molecular weight polycyclic aromatic hydrocarbons: a review of the microbial degradation of benzo[a]pyrene, Int. Biodet. & Biodegr. 45 (2000) 57-88.

[3] R. Kanaly, S. Harayama, Biodegradation of High-Molecular-Weight Polycyclic Aromatic Hydrocarbons by Bacteria, J. Bacteriol. 182 (2000) 2059-2067.

[4] S. Demaneche, C. Meyer, J. Micoud, M. Louwagie, J.C. Willison, Y. Jouanneau, Identification and functional analysis of two aromatic-ring-hydroxylating dioxygenases from a *Sphingomonas* strain that degrades various polycyclic aromatic hydrocarbons, App. Environment. Microbiol. 70 (2004) 6714-6725.

[5] Y. Jouanneau, C. Meyer, J. Jakoncic, V. Stojanoff, J. Gaillard, Characterization of a Naphthalene Dioxygenase Endowed with an Exceptionally Broad Substrate Specificity toward Polycyclic Aromatic Hydrocarbons, Biochemistry 45 (2006) 12380-12391.

[6] B. Kauppi, K. Lee, E. Carredano, R.E Parales, D.T. Gibson, H. Eklund, S. Ramaswamy, Structure of an aromatic-ring-hydroxylating dioxygenase-naphthalene 1,2-dioxygenase, Structure 6 (1998) 571–586.

[7] L. Gakhar, Z.A. Malik, C.C.R. Allen, D.A. Lipscomb, M.J. Larkin, S. Ramaswamy, Structure and Increased Thermostability of *Rhodococcus* sp. Naphthalene 1,2-Dioxygenase, J. Bacteriol. 197 (2005) 7222-7231.

[8] D.J. Ferraro, L. Gakhar, S. Ramaswamy, Rieske business: Structure–function of Rieske non-heme oxygenases, Biochemical and Biophysical Research Communications 338 (2005) 175–190.

[9] N.E. Chayen, A novel technique to control the rate of vapour diffusion, giving larger protein crystals, J. Appl. Cryst. 30 (1997) 198-202.

[10] M. Allaire, M. Aslantas, A. Berntson, L. Bermann, S. Cheung, B. Clay, R. Greene, J. Jakoncic, E. Johnson, C.C. Kao, A. Lenhard, S. Pjerov, D.P. Siddons, W. Stober, V. Venkatagiriyappa, Z. Yin, V. Stojanoff, Synchrotron Radiation News 16 (2003) 20-25.

[11] X. Dong, S. Fushinobu, E. Fukuda, T. Terada, S. Nakamura, K. Shimizu, H. Nojiri, T. Omori, H. Shoun, T. Wakagi, Crystal structure of the terminal oxygenase component of cumene dioxygenase from *Pseudomonas fluorescens* IP01, J. Bacteriol. 187 (2005) 2483-2490.

[12] G.N. Murshudov, A.A. Vagin, E.J. Dodson, Refinement of Macromolecular Structures by the Maximum-Likelihood Method, Acta Cryst. D53 (1997) 240-255.

[13] P. Emsley, K. Cowtan, Coot: Model-Building Tools for Molecular Graphics, Acta. Cryst. D60 (2004) 2126-2132.

[14] J. Liang, H. Edelsbrunner, C. Woodward (1998) Anatomy of Protein Pockets and Cavities: Measurement of Binding Site Geometry and Implications for Ligand Design, Protein Science, 7, 1884-1897.

[15] Y. Furusawa, V. Nagarajan, M. Tanokura, E. Masai, M. Fukuda, T. Senda, Crystal Structure of the Terminal Oxygenase Component of Biphenyl Dioxygenase Derived from *Rhodococcus* sp. Strain RHA1, J. Mol. Biol. 342 (2004) 1041-1052.

[16] B.M. Martins, T. Svetlitchnaia, H. Dobbek, 2-Oxoquinoline 8-Monooxygenase Oxygenase Component: Active Site Modulation by Rieske-[2Fe-2S] Center Oxidation/Reduction, Structure 13 (2005) 817-824.

[17] H. Nojiri, Y. Ashikawa, H. Noguchi, J.W. Nam, M. Urata, Z. Fujimoto, H. Uchimura, T. Terada, S. Nakamura, K. Shimizu, T. Yoshida, H. Habe, T. Omori, Structure of the terminal oxygenase component of angular dioxygenase, carbazole 1,9a-dioxygenase, J. Mol. Biol. 351 (2005) 355-370.

[18] Nam, J.W., Nojiri, H., Yoshida, T., Habe, H., Yamane, H., Omori, T. (2001) New Classification System for Oxygenase Components Involved in Ring-Hydroxylating Oxygenations, Biosci. Biotechnol. Biochem. 65, 254-263

[19] R.E. Parales, The role of active-site residues in naphthalene dioxygenase, J. Ind. Microbiol. Biotechnol. 30 (2003) 271–278.

[20] R.E. Parales, S.M. Resnick, C. Yu, D.R. Boyd, N.D. Sharma, D.T. Gibson, Regioselectivity and Enantioselectivity of Naphthalene Dioxygenase during Arene *cis*-Dihydroxylation: Control by Phenylalanine 352 in the α–Subunit, J. Bacteriol. 182 (2000) 5495-5504.

[21] R. Friemann, M.M. Ivkovic-Jensen, D.J. Lessner, C. Yu, D.T. Gibson, R.E. Parales, H. Eklund, S. Ramaswamy, Structural Insight Into the Dioxygenation of Nitroarene Compounds: The Crystal Structure of Nitrobenzene Dioxygenase, J. Mol. Biol. 348 (2005) 1139-1151.

[22] W.L. DeLano, DeLano Scientific, San Carlos, CA, USA, 2002.

[23] R.M. Esnouf, Journal of Molecular Graphics 15 (1997) 132-134.

[24] P.J. Kraulis, J. Appl. Cryst. 24 (1991) 946-950.

[25] E.A. Merritt, M.E. Murphy, Raster3D Version 2.0: A Program for Photorealistic Molecular Graphics, Acta Cryst. D50 (1994) 869-873.

Table 1. Residues lining the catalytic pocket of dioxygenases of known structure.

(footnote) Relative position to the catalytic Fe: D, distal; C, central and P, proximal. (--) no structurally equivalent residues were observed. Substrate free structures were used in the comparison [6,16,7,12,15,17,18].

Figure Legends

Fig. 1. Structure of the αβ heterodimer of PhnI: the α-subunit is shown in grey, catalytic domain, and in pink, Rieske domain, the β-subunit is shown in yellow. The surface of the substrate binding pocket is shown in the foreground; loops LI and LII are indicated. The Rieske domain of the adjacent α-subunit is shown in cyan. This view emphasizes important features of the enzyme, especially the proximity of the 2Fe-2S cluster and the mononuclear Fe at the interface between two adjacent α-subunits. The figure was produced with Pymol [22].

Fig. 2. Close view of the active site showing the residual positive density modeled as an indole molecule. Four maps are shown: 2fo-fc contoured at the 1σ level, in grey and the fo-fc at the +3σ, iņgreen after addition of the indole molecule; and the respective Omit maps, 2fo-fc at 1σ, in cyan and fo-fc at 3σ, in red. fo-fc maps contoured at the -3σ levęldid not present any residual density and are not shown. In this configuration, the C3 atom of indole is located 2 Å from the closest water molecule, in red, which is 2.6 Å from the mononuclear Fe atom shown in green and at 2.2 Å from the second coordinated water molecule. The figure was produced with BOBSCRIPT [23,24] and Raster3D [25].

Fig. 3. The PhnI active site with a BaP substrate modeled in the catalytic pocket. (a) Residues shown in front, relative to the substrate (in green) are labeled in black and residues in the back are labeled in grey. With the exception of Gly 205, only side chains are represented. The mononuclear Fe is represented as a red ball. (b) Surface plot of the PhnI substrate cavity showing the substrate in the same orientation exposing C9 and C10 towards the mononuclear iron.

Fig. 4. The catalytic pocket for PhnI (upper panel), NDO-O_{9816-4} (central panel) and BPDO-O_{RHA1} (lower panel), is shown on the left in its substrate free form and on the right for the substrate bound enzyme complexes. For each of the dioxygenases represented the comparison between the left and right panels shows the changes in the catalytic pocket upon substrate binding. The structures for NDO-O_{9816-4} and BPDO-O_{RHA1} on the right were obtained using the coordinates of the substrate-bound enzyme complexes (PDB access code 1O7G and 1ULJ, respectively). For PhnI, the cavity shown on the right was obtained after rotation of side chains of residues, Leu 223 and Phe 350, taking into account steric constrains due to van der Waals contacts. With these minor conformational changes BaP can only fit in the PhnI pocket in the orientation shown. In this orientation BaP would be hydroxylated in position 9,10- consistent with biochemical assays [5]. The figure was produced with Pymol [22].

Figure 1

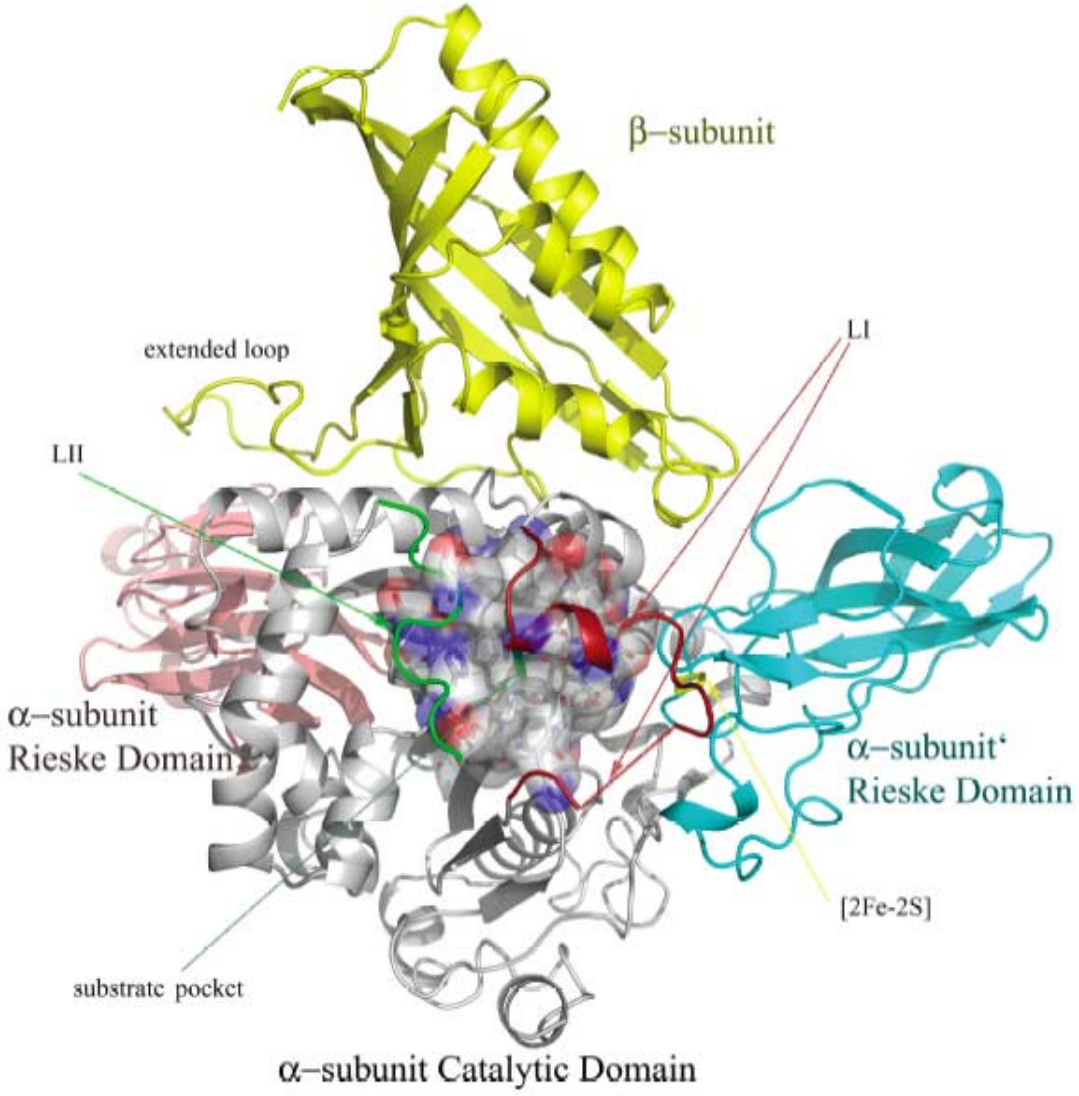
β–subunit
extended loop
LI
LII
α–subunit
Rieske Domain
α–subunit'
Rieske Domain
[2Fe-2S]
substrate pocket
α–subunit Catalytic Domain

Figure 2

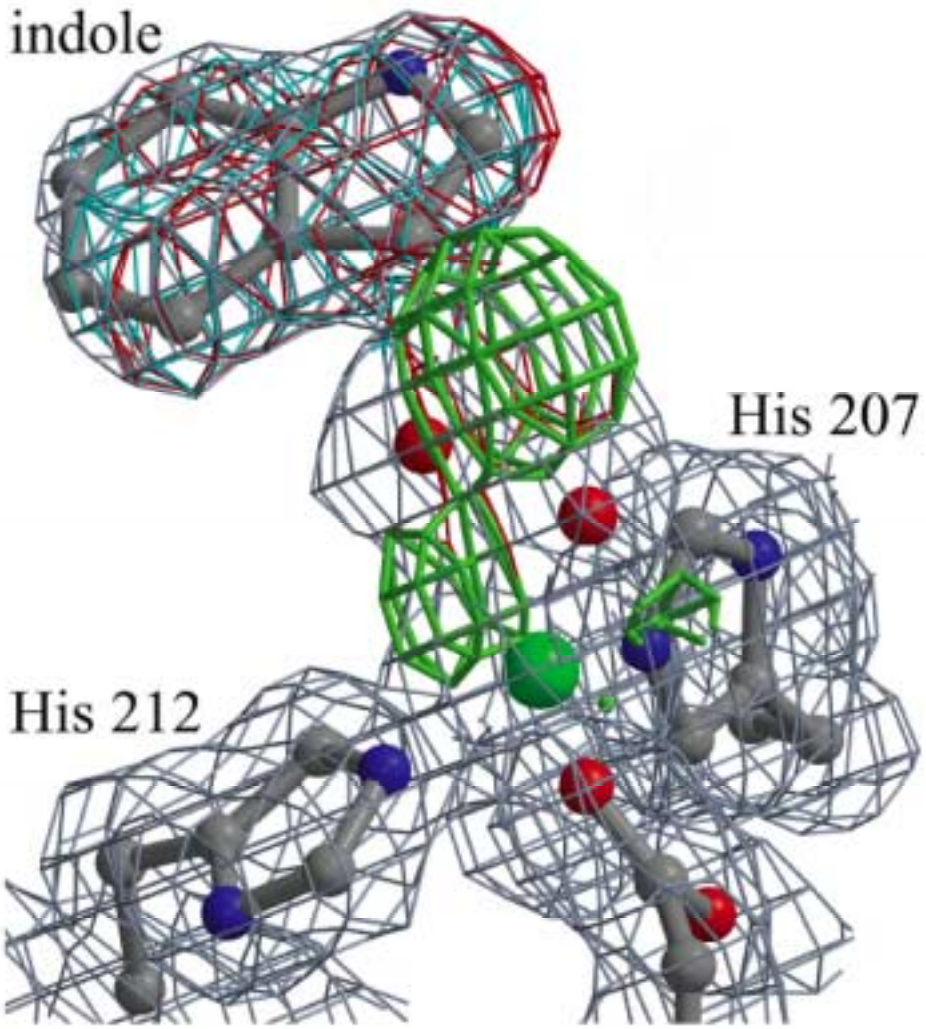

Figure 3

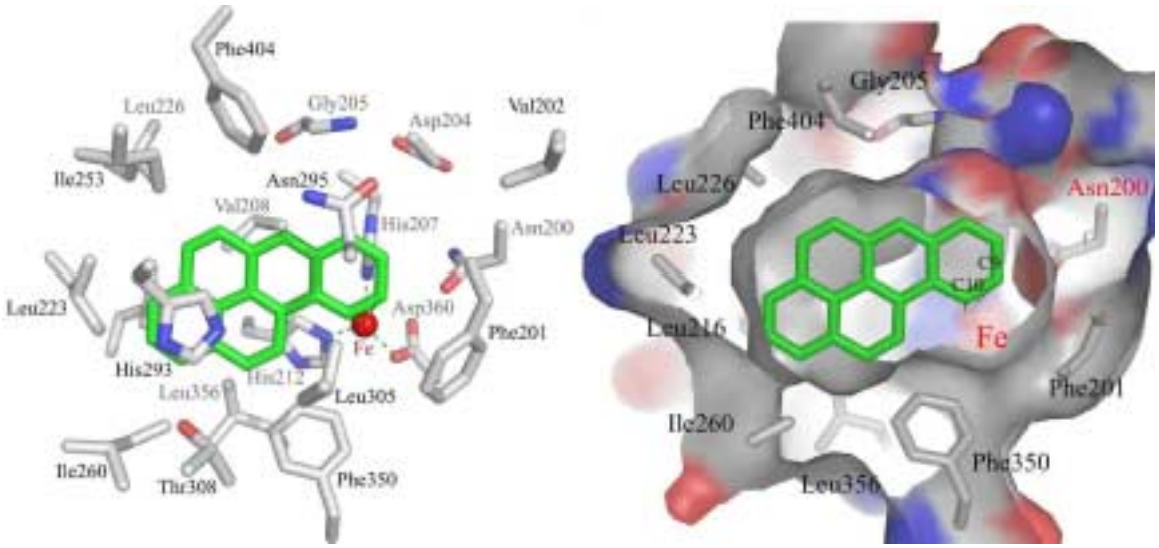
Phe404
Leu226
Gly205
Asp204
Val202
Ile253
Asn295
Val208
His207
Asn200
Leu223
Asp360
Phe201
Fe
His293
His212
Leu356
Leu305
Ile260
Thr308
Phe350
Gly205
Phe404
Leu226
Asn200
Leu223
Fe
Leu216
Phe201
Ile260
Phe350
Leu356

Figure 4

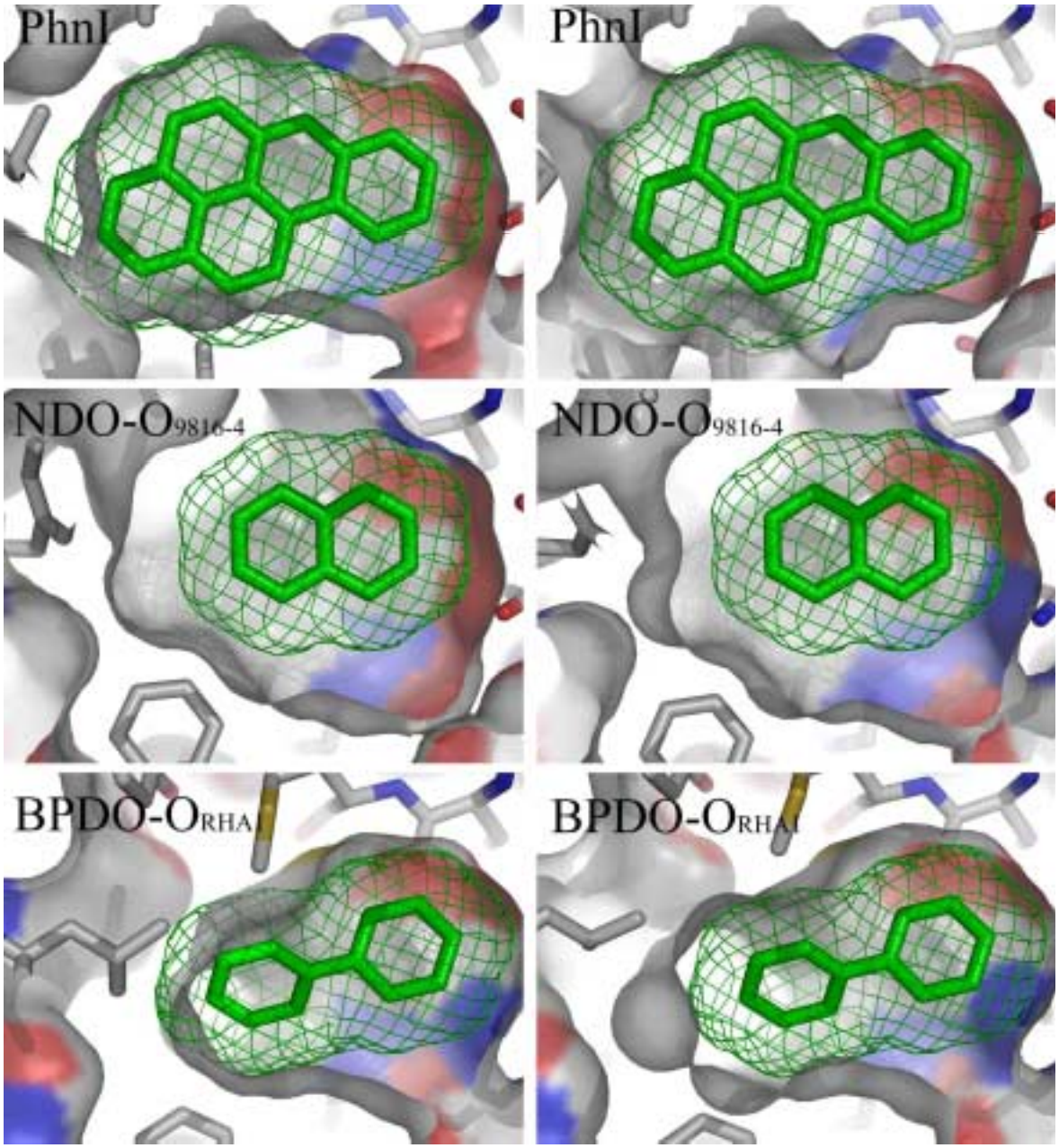

Table 1. Residues lining the catalytic pocket of dioxygenases of known structure.

	GroupI				GroupII		GroupIII	
	PhnI	**NDO-O_{9816-4}**	**NBDO-O_{JS765}**	**NDO-O_{12038}**	**CDO-O_{IPO1}**	**BPDO-O_{RHA1}**	**OMO-O_{86}**	**CARDO-O_{CA10}**
P	Asn200	Asn201	Asn199	Asn209	Gln227	Gln217	Asn215	Asn177
P	Phe201	Phe202	Phe200	Phe210	Phe228	Phe218	Leu302 Gly216	Leu207 Gly178
P	Val202	Val203	Val201	Val211	Cys229	Cys219	Phe217 Val296	Phe179 Ile264
C	Gly203	Gly204	Gly202	Gly212	Ser230	Ser220	Gln264 Phe217	--------
C	Gly205	Ala206	Gly204	Ala214	Met232	Met222	Asn219	Pro181
C	Val208	Val209	Val207	Thr217	Ala235	Ala225	Ile222	Ile184
C	Leu216	Leu217	Leu215	Val225 Ala230	Val244	Val234	Leu238	Val193 Leu200
D (LI)	Leu223	Phe224	Leu222	Phe293	Leu284	Leu274	Val231	Ala199
D (LI)	Leu226	Leu227	Leu225	Phe236	Leu259	------	Pro239	Pro201
C	Gly251	Gly251	Gly249	Gly252	Gly276	Gly266	-------	Ile262 Asp229
D (LII)	Ile253	Leu253	Phe251	Ile254	Phe278	Tyr268	Tyr292 Phe267	--------
D (LII)	Ile260	Val260	Asn258	Met309	Ile288	Ile278	Trp307	--------
C	His293	His295	Phe293	Phe293	Ala321	Ala311	Tyr292	Ala259
P	Asn295	Asn297	Asn295	His295	His323	His313	Thr294	Ile262
C	Leu305	Leu307	Leu305	Phe307 Gly305	Leu333	Leu323	Gln314 Val304	Val272
C	Thr308	Ser310	Ser308	Phe320 Phe307	Ile336	Ile326	Trp307	Phe275
C	Phe350	Phe352	Ile350	Phe362	Phe378	Phe368	Asn362	Asn330 Phe275
C	Leu356	Trp358	Trp356	Phe368	Tyr384	Tyr374	Phe361	Phe329
C	Phe404	Ala407	Phe251 Ala405	Asp418	Met227 Phe273	Met222 Val422	Leu266 Asn219	---------
	Identity(%)	63	47	37	37	32	11	5

(Table 1) Relative position to the catalytic Fe: D, distal; C, central and P, proximal. (--) no structurally equivalent residues were observed. Substrate free structures were used in the comparison [6,16,7,12,15,17,18].